RESEARCH ARTICLE

A New Method for Locating Positions of Single-Core Cables in Three-Phase Submarine Power Circuits Based on Phase Difference Data

YIRAN CHEN[1], SHANGQING LIANG [1,2], GUOQING YANG [1,2], LIN WANG [1], YUANGUO ZHOU [3], AND XIAOQING TIAN[2,4]

[1]College of Electronics and Information, Hangzhou Dianzi University, Hangzhou 310018, China
[2]Ocean Technology and Equipment Research Center, Hangzhou Dianzi University, Hangzhou 310018, China
[3]College of Communication and Information Engineering, Xi'an University of Science and Technology, Xi'an 710054, China
[4]School of Mechanical Engineering, Hangzhou Dianzi University, Hangzhou 310018, China

Corresponding author: Shangqing Liang (liangshangqing@hdu.edu.cn)

ABSTRACT The identification of submarine cable locations is crucial for their operation and maintenance. Precise location data enables the monitoring of route changes and facilitates rapid fault detection. Magnetic sensing is commonly used for detecting buried submarine cables. However, current research seldom discusses the impact of mutual magnetic field interference among submarine power cables on location accuracy and considers only the magnetic field intensity for cable detection. In this study, the authors first establish a general magnetic field model for three parallel single-core submarine power cables carrying three-phase currents and thoroughly investigate the variations in the amplitude and phase difference of the magnetic field surrounding the cables. Based on this model, the authors introduce a gradient measurement method based on the phase difference for the first time and compare its location accuracy with that of the traditional extremum method. Our findings reveal that the phase difference method offers higher location accuracy at longer detection distances, whereas the extremum method is preferable for shorter distances because of its simpler device and criteria.

INDEX TERMS Magnetic field analysis, magnetic sensing, phase difference measuring, submarine power cable location.

I. INTRODUCTION

As marine economies expand, submarine cables have become increasingly important for power transmission and communication [1]. With the growing use of submarine cables, the risk of damage from human activities and environmental factors has increased [2]. Consequently, regular surveys of submarine cables are essential to monitor route changes and swiftly locate faults when damage occurs [3]. Common submarine cable location methods include visual tracking [3]; hydroacoustic detection [3], [4], [5]; and magnetic

The associate editor coordinating the review of this manuscript and approving it for publication was Tao Wang [ID].

sensing [6], [7], [8]. Magnetic sensing is the most suitable method for submarine power cables because they are typically buried in the seabed, limiting the effectiveness of visual tracking and hydroacoustic detection [8]. Owing to the large AC currents transmitted through the cables, an AC magnetic field is generated around them, enabling their detection using AC magnetic sensors such as search coils [9]. The extremum method, which is based on the AC magnetic field intensity, is a common passive method in the industry [10]. Considering the magnetic field model of a single submarine cable, the maximum detected value of the horizontal magnetic field intensity and the minimum detected value of the vertical magnetic field intensity occur when magnetic sensors are

directly above the cable [6]. Hence, the cable can be located based on the positions of the extremums. Thus, the cable location can be determined by identifying extremums. This method is easy to implement, and the equipment can be mounted on a ship rather than on an unmanned underwater vehicle (UUV) in shallow water. However, this method is susceptible to measurement noise from sensors and external magnetic field disturbances, owing to the gradual change in the magnetic field intensity near the extremum. Another common method involves the use of multiple magnetic sensors with fixed relative positions to analyze the location and burial depth of the cable. This method can achieve cable tracking instead of sweeping surveys, typically employing a diver or UUV to ensure a short detection distance [11], [12]. Among the current magnetic sensing methods, the impact of mutual magnetic field interference among submarine power cables on location accuracy has been scarcely researched, and cable location only considers the magnetic field intensity [13], [14].

In this study, a general magnetic field model for three parallel single-core submarine power cables carrying three-phase currents is first established. The amplitude and phase difference variations between the horizontal and vertical components of the magnetic flux density surrounding the cables are investigated thoroughly. Our research indicates that the magnetic field distribution around each cable is significantly altered by mutual interference from other cables, and is affected by the conductivity of the surrounding medium. As the conductivity increases, the wavelength of the AC magnetic field shortens and becomes comparable to the distance between the source and probe point. Consequently, phase variations due to different spatial distances cannot be ignored, resulting in a non-axisymmetric magnetic field distribution, which decreases the location accuracy. The authors then propose a gradient measurement method based on the phase difference for the first time and thoroughly discuss the location accuracy comparisons between the extremum and phase difference methods. Our results show that the phase difference method provides a higher location accuracy when the probe height is high. Finally, the proposed model is validated using a simple laboratory device and compared with the finite element method (FEM). The remainder of this paper is organized as follows: In Section II, a theoretical analysis of the general magnetic field model for single-core cables in three-phase submarine power circuits is provided. In Section III, the authors discuss the distributions of the AC magnetic field intensity and phase difference separately. A gradient measurement method based on the phase difference for the cable location is then proposed. Building on this, the authors present comparisons of the location accuracy between the extremum method and the phase difference method, considering different probe heights and conductivities of environmental media. In Section IV, a simple laboratory device to validate the reliability of the proposed method is set up and the results of the phase difference distributions obtained using the proposed model and the

FEM-based model are compared. Finally, Section V presents our conclusions.

II. GENERAL MAGNETIC FIELD MODEL

In this general magnetic field model, the single-core cables in three-phase submarine power circuits are simplified as three parallel, horizontally-aligned, long straight lines carrying phase currents A, B, and C. Although most submarine cables contain a metallic sheath, their shielding effect for the AC magnetic field at the power frequency can be ignored. This is because the metallic sheath is typically composed of several stranded steel wires, which cannot effectively shield the power frequency magnetic field. The relative positions of the cables and probe point P are shown in Figure 1. A rectangular coordinate system is established with the origin coordinate located at the position of the phase current B, and the positive directions of the coordinate axes are depicted in Figure 1. The cable carrying phase current A is located at coordinates $(L_1, 0)$, whereas the cable carrying phase current C is located at coordinates $(L_2, 0)$. The probe point P is located at coordinates (x, h).
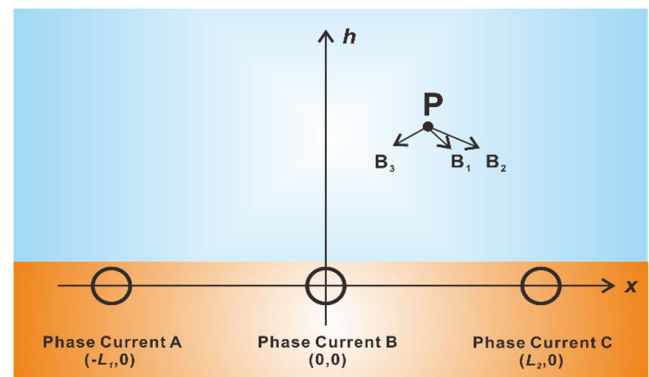

FIGURE 1. The rectangular coordinate system used in general magnetic field model.

The magnetic fields generated by the phase currents A (I_1), B (I_2), and C (I_3) at probe point P can be expressed from the appropriate Maxwell's equations [15], [16], [17], [18]:

$$B_1 = \frac{\gamma \mu I_1 K_1(\gamma R_1)}{2\pi} \left[\frac{h}{R_1} e_p + \frac{(x + L_1)}{R_1} e_v \right] \quad (1)$$

$$B_2 = \frac{\gamma \mu I_2 K_1(\gamma R_2)}{2\pi} \left(\frac{h}{R_2} e_p + \frac{x}{R_2} e_v \right) \quad (2)$$

$$B_3 = \frac{\gamma \mu I_3 K_1(\gamma R_3)}{2\pi} \left[\frac{h}{R_3} e_p + \frac{(x - L_2)}{R_3} e_v \right] \quad (3)$$

where R_1 is the distance between phase current A and probe point P, R_2 is the distance between phase current B and probe point P, R_3 is the distance between phase current C and probe point P, μ is the permeability of seawater, e_p is the unit vector in the x direction, e_v is the unit vector in the h direction, $K_1(\gamma R)$ is the modified Bessel function of the second kind of order 1, and γ is the propagation constant which can be

expressed as

$$\gamma = (1+i)\sqrt{\pi f \mu \sigma} \tag{4}$$

where σ is the conductivity of seawater.

The total magnetic field (B) at the probe point P can be expressed as follows:

$$B = B_1 + B_2 + B_3 = B_p e_p + B_v e_v \tag{5}$$

where B_p and B_v represent the horizontal and vertical components of the total magnetic field, respectively, and are expressed as complex sinusoids with frequency f:

$$B_p = A_p e^{i(2\pi f t + \theta_p)} \tag{6}$$

$$B_v = A_v e^{i(2\pi f t + \theta_v)} \tag{7}$$

where A_p and A_v are amplitude components, θ_p and θ_v are phase components.

III. THEORETICAL ANALYSIS AND DISCUSSIONS

In this section, the amplitude and phase difference distributions of the AC magnetic field around three-phase submarine power cables using the general model discussed earlier are calculated. Then, the common extremum method and the phase difference gradient measurement method are compared. Here, balanced phase currents with an amplitude equal to that of I_0 are considered. According to the actual situations of submarine power cables in the Ningbo-Zhoushan sea area of China and the selection principles of the marine cable route [19], some parameters of the model in this section are as follows:

$$\begin{cases} I_0 = 500\text{A} \\ L_1 = L_2 = 50\text{m} \\ \mu = \mu_0 = 4\pi \times 10^{-7}\text{H/m} \end{cases} \tag{8}$$

and the initial conditions of phase currents are

$$\begin{cases} I_1|_{t=0} = I_0 \\ I_2|_{t=0} = I_0 e^{-\frac{2}{3}\pi i} \\ I_3|_{t=0} = I_0 e^{\frac{2}{3}\pi i} \end{cases} \tag{9}$$

A. AMPLITUDE DISTRIBUTION

The amplitudes of the horizontal component (A_p) and vertical component (A_v) around the cables are analyzed using (6) and (7). The variations in amplitude with position at different heights (h) are shown in Figure 2. The surrounding medium is set as seawater with conductivity (σ) equal to 4S/m [20].

When probe point P moves nearly above the cables, A_p reaches its maximum and A_v reaches its minimum. This characteristic is typically used for cable location by detecting the positions of extremum values, which is referred to as the extremum method. An evident advantage of this method is that it is an intuitive criterion that does not require complex data processing. However, as shown in Figure 2, this method has two disadvantages in terms of the location accuracy. First, the positions of the minimum values shift significantly with increasing height (h) owing to the mutual interference of the
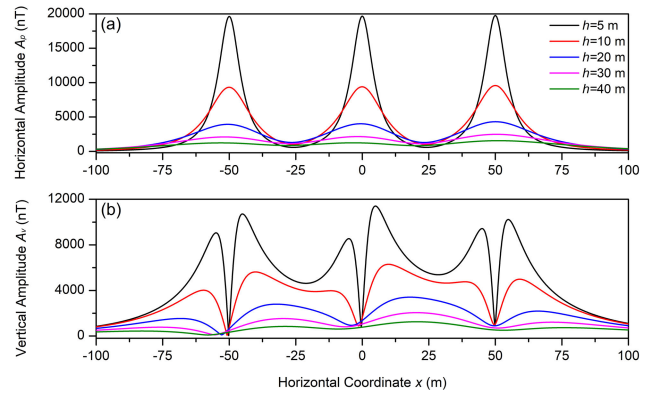

FIGURE 2. Variations in amplitudes of magnetic field with position at different heights (h). (a) The amplitude of the horizontal component (A_p). (b) The amplitude of the vertical component (A_v).

three cables. Second, the amplitude variation of the magnetic field is gradual near the extremum values. Therefore, the measurement noise from sensors or external magnetic field disturbances may affect the judgment of the positions of the extremum values. Further research on location accuracy is discussed in Part C of this section.

Additionally, the variations in the different surrounding media are compared in Figure 3. When the surrounding medium is freshwater, the conductivity (σ) is set as 0.01 S/m [21]. When the surrounding medium is seawater with a lower salt concentration, the conductivity (σ) is set as 1 S/m. The vertical coordinate (h) is set as 10 m.
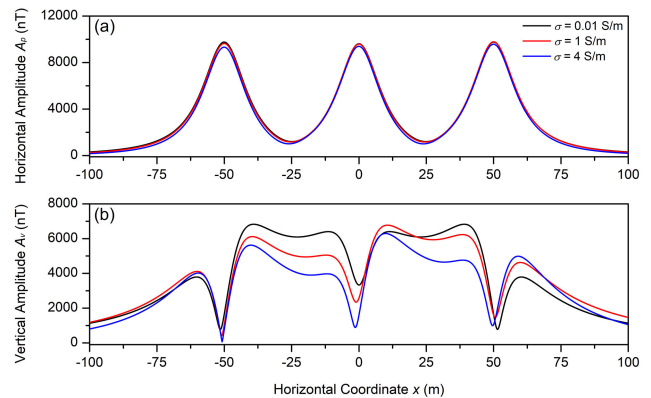

FIGURE 3. Variations in amplitudes with different surrounding media. (a) The amplitude of the horizontal component (A_p). (b) The amplitude of the vertical component (A_v).

The results show that increasing conductivity disrupts the axial symmetry of the curves. As the conductivity of the surrounding medium increases, the wavelength of the AC magnetic field decreases. The wavelength (λ) of the AC magnetic field in the conductive medium can be calculated by the following formula:

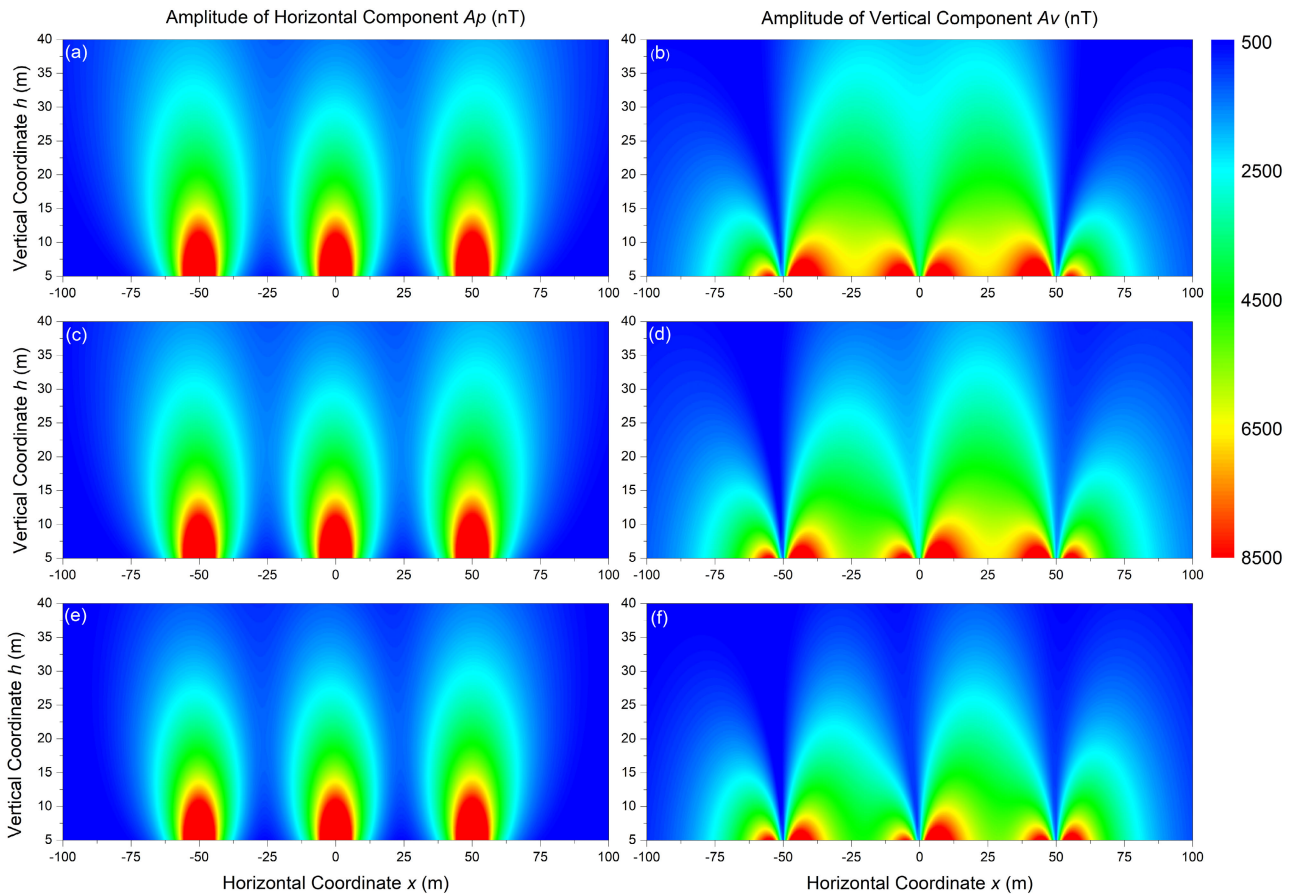$$\lambda = \frac{2\pi}{\sqrt{\pi f \mu \sigma}} \tag{10}$$

FIGURE 4. Amplitude distributions with different conductivities. (a) The amplitude of the horizontal component (A_p) with $\sigma = 0.01$ S/m. (b) The amplitude of the vertical component (A_v) with $\sigma = 0.01$ S/m. (c) The amplitude of the horizontal component (A_p) with $\sigma = 1$ S/m. (d) The amplitude of the vertical component (A_v) with $\sigma = 1$ S/m. (e) The amplitude of the horizontal component (A_p) with $\sigma = 4$ S/m. (f) The amplitude of the vertical component (A_v) with $\sigma = 4$S/m.

Consequently, the wavelength of the AC magnetic field with a frequency of 50 Hz is reduced to approximately 220 m in seawater ($\sigma = 4$ S/m) compared with the wavelength of 6000 km in air or vacuum. In this case, the distances between the sources (phase currents A, B, and C) and probe point are comparable to the wavelength. The phase variations caused by different spatial distances cannot be ignored, resulting in the non-axisymmetric phenomenon observed in Figure 3. More detailed amplitude distributions for different conductivities are presented in Figure 4.

B. PHASE DIFFERENCE DISTRIBUTION

The phase difference ($\Delta\theta$) between the horizontal component (B_p) and vertical component (B_v) of the AC magnetic field can be expressed as

$$\Delta\theta = \theta_p - \theta_v \tag{11}$$

The variations in the phase difference with position at different heights (h) are shown in Figure 5.

The results demonstrate that the phase differences near the positions directly above the phase currents A, B, and C change rapidly. The sensitive variations in the phase
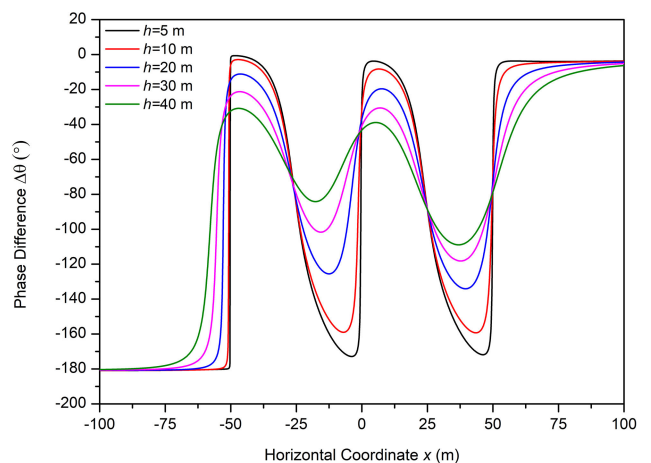

FIGURE 5. Variations in phase difference ($\Delta\theta$) of magnetic field with position at different heights (h).

difference with position can reduce the influence of detection noise and environmental noise, as validated in Part C of this section. The effect of the conductivity on the phase difference is displayed in Figure 6, and more detailed phase difference
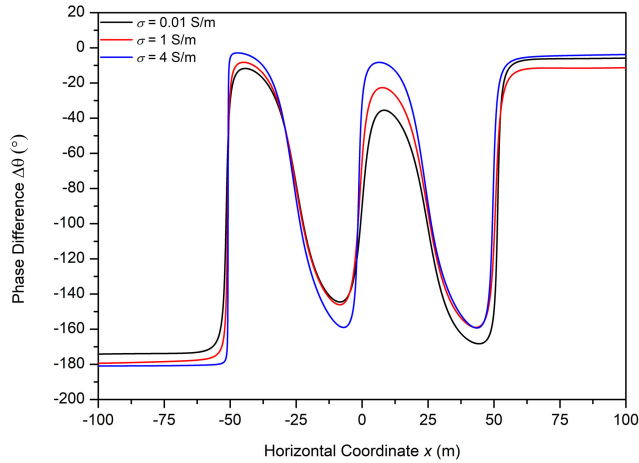
FIGURE 6. Variations in phase differences ($\Delta\theta$) with different surrounding media.
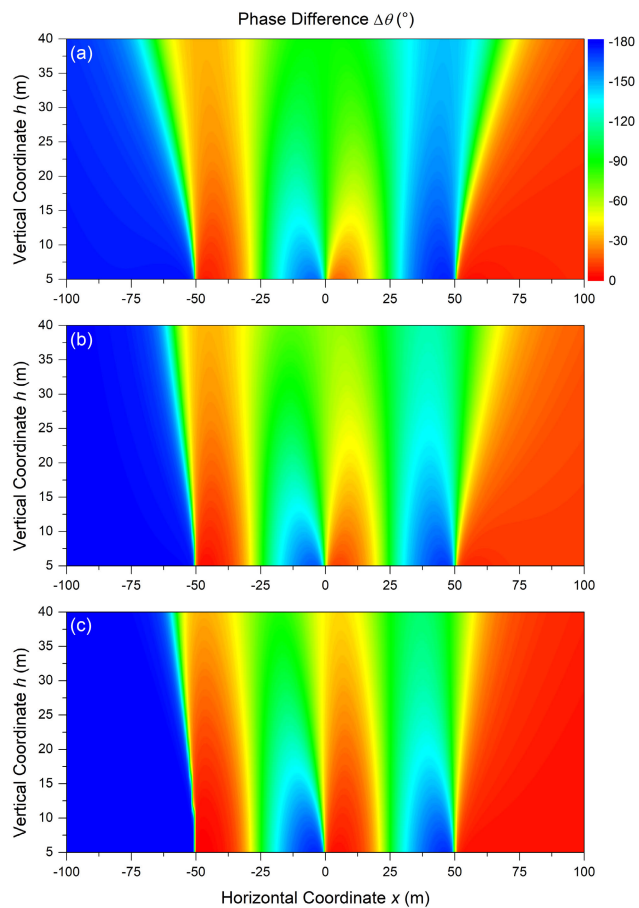

FIGURE 7. Phase difference distributions with different conductivities. (a) The variations of phase difference ($\Delta\theta$) with $\sigma = 0.01$ S/m. (b) The variations of phase difference ($\Delta\theta$) with $\sigma = 1$ S/m. (c) The variations of phase difference ($\Delta\theta$) with $\sigma = 4$ S/m.

FIGURE 8. Variations in gradient of phase difference with position at different heights (h). The black line represents the gradient values of the phase differences in the $h = 5$ m subtracted from those in the $h = 8$ m. The red line represents the gradient values of the phase differences in the $h = 10$ m subtracted from those in the $h = 13$ m. The blue line represents the gradient values of the phase differences in the $h = 20$ m subtracted from those in the $h = 23$ m. The pink line represents the gradient values of the phase differences in the $h = 30$ m subtracted from those in the $h = 33$ m. The green line represents the gradient values of the phase differences in the $h = 40$ m subtracted from those in the $h = 43$ m.

Similar to the use of extremum values to identify cables in the extremum approach, a clear criterion is required for implementation in actual applications. However, the results show that the phase differences near the positions directly above the cables are not suitable criteria. Therefore, a gradient measurement method in the vertical direction is proposed. In this method, two probe points with the same horizontal coordinates and different vertical coordinates are used to detect the phase differences simultaneously. The phase differences of the two probe points are then subtracted to obtain the gradient value. The vertical coordinate difference is set to 3 m in this study, and the related results are shown in Figure 8.

The results indicate that the gradient values near the positions directly above the cables are close to zero with steep slopes. Hence, the positions of the zero-crossing points can be regarded as the cable positions. This characteristic can be used as the criterion for cable location in the phase difference detection method.

C. COMPARISIONS OF TWO METHODS

In this part, the location accuracies of the two methods are compared. The location accuracy (ε) can be expressed as

$$\varepsilon = \Delta x + \delta_d \quad (12)$$

where Δx is the model bias and δ_d is the detection error. Model bias is a type of systematic bias caused by the theoretical models and methods. It represents the differences between the positions determined by the criterion and the true positions of the cables. In the extremum method, the positions determined by the criterion are the positions of the extremum values, whereas in the proposed method, they are the positions of the zero-crossing points. The detection error is caused by the detection noise of the sensors and

distributions with different conductivities are presented in Figure 7. It can be observed that the central symmetries of the curves are disrupted with increasing conductivity. The reason for this is similar to that shown in Figure 3.
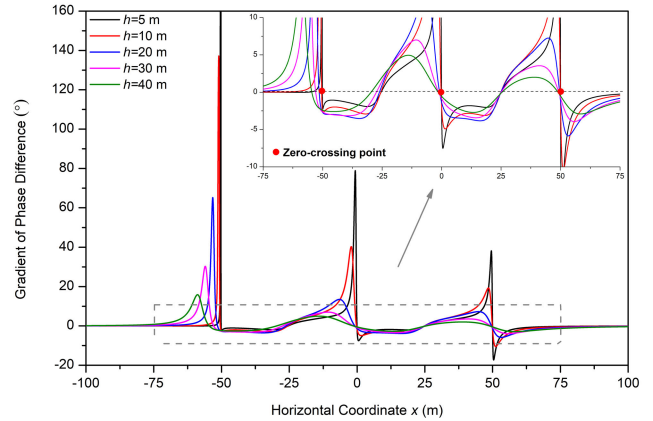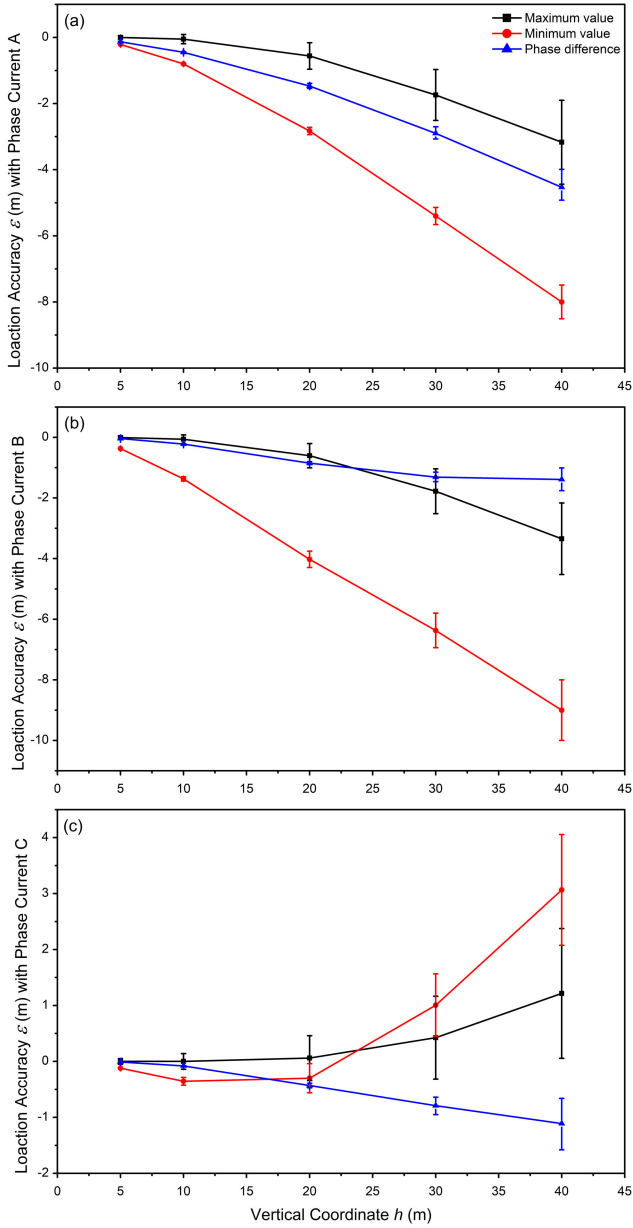
FIGURE 9. Comparisons of location accuracy with $\sigma = 4$ S/m. The solid symbols represent model biases and the error bars represent detecion errors. (a) Location accuracy with phase current A. (b) Location accuracy with phase current B. (c) Location accuracy with phase current C.

FIGURE 10. Comparisons of location accuracy with $\sigma = 1$ S/m. The solid symbols represent model biases and the error bars represent detection errors. (a) Location accuracy with phase current A. (b) Location accuracy with phase current B. (c) Location accuracy with phase current C.

the environmental noise. For ease of analysis, the detection noise of the sensors and environmental noise can be treated as total amplitude noise (N_B). The detected amplitudes of the magnetic field can be expressed as

$$A_{pm} = A_p \pm N_B \qquad (13)$$

$$A_{vm} = A_v \pm N_B \qquad (14)$$

where A_{pm} is the detected amplitude of the horizontal magnetic field and A_{vm} is the detected amplitude of the vertical magnetic field. In the phase difference method, amplitude noise is converted to phase noise. In the phase difference method, amplitude noise is converted to phase noise. The time difference between the zero crossings of the sinusoidal
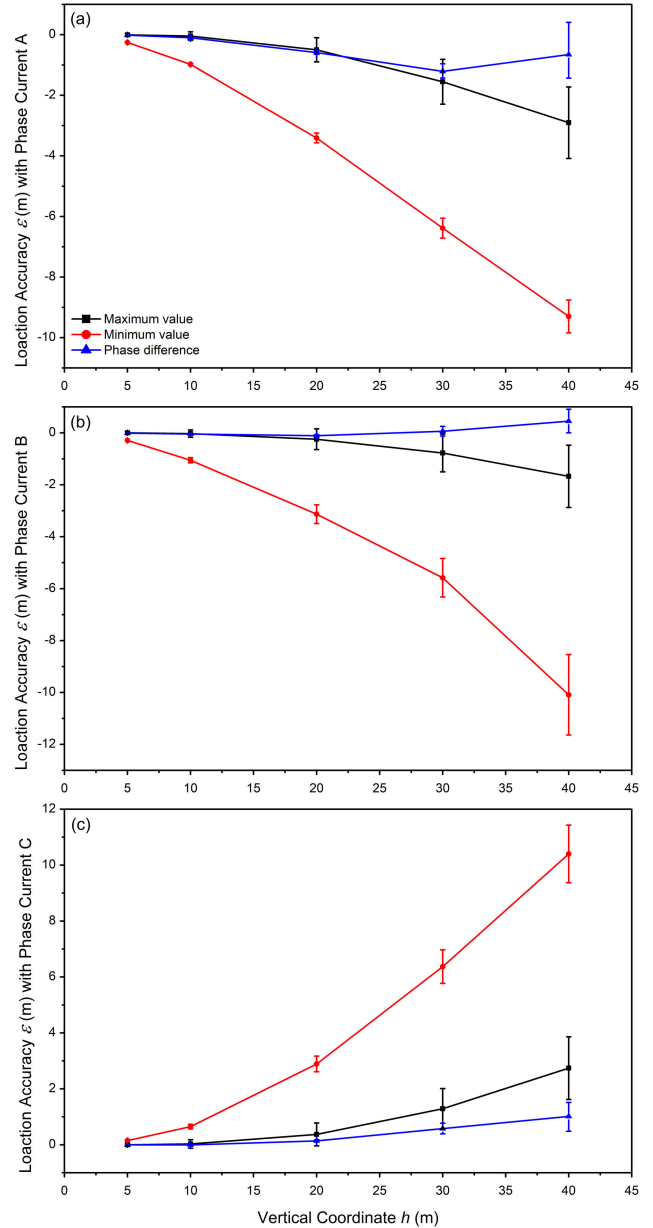
signals is measured to calculate the phase difference. Consequently, the detected phase difference ($\Delta\theta_m$) can be expressed as:

$$\Delta\theta_m = (\theta_p \pm N_{p\theta}) - (\theta_v \pm N_{v\theta}) = \Delta\theta \pm N_{p\theta} \mp N_{v\theta} \quad (15)$$

where

$$N_{p\theta} = \arcsin(\frac{N_B}{A_p}) \approx \frac{N_B}{A_p} \quad N_B \ll A_p \qquad (16)$$

$$N_{v\theta} = \arcsin(\frac{N_B}{A_v}) \approx \frac{N_B}{A_v} \quad N_B \ll A_v \qquad (17)$$

In practical applications, the detection noise of sensors and the precise seawater conductivity cannot be predicted
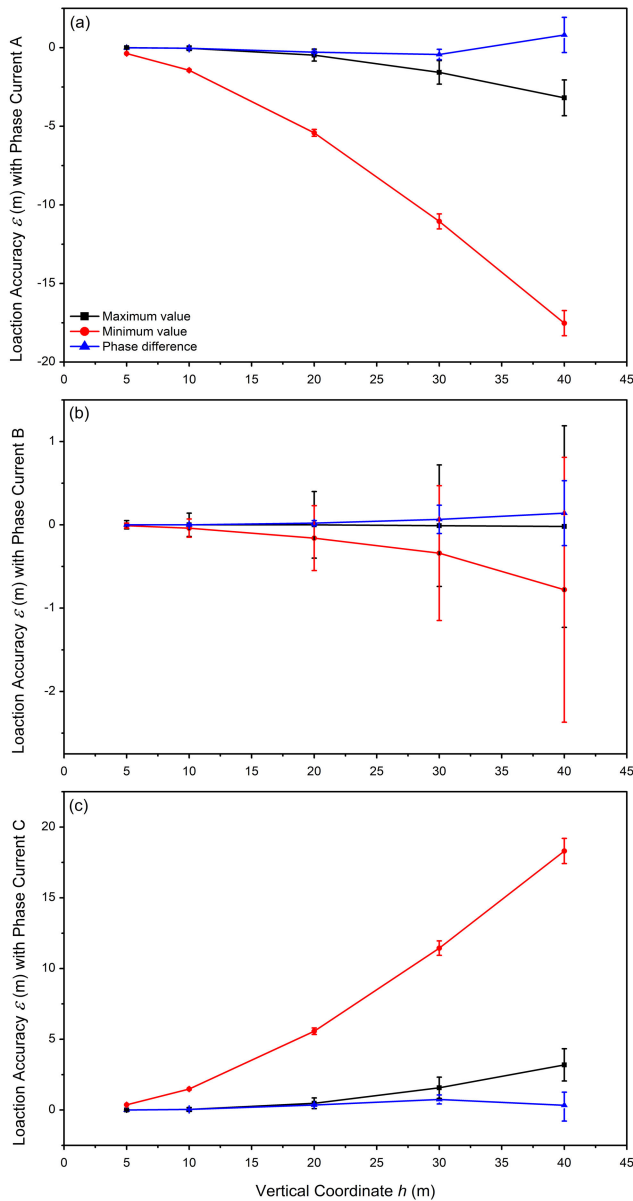
FIGURE 11. Comparisons of location accuracy with $\sigma = 0.01$ S/m. The solid symbols represent model biases and the error bars represent detection errors. (a) Location accuracy with phase current A. (b) Location accuracy with phase current B. (c) Location accuracy with phase current C.

the positions directly above the phase currents. Second, the model bias of the extremum method using minimum values is too large, resulting in a much lower location accuracy compared with other methods. Third, the location accuracy of the extremum method using maximum values is close to that of the phase difference method at small h values but lower at large h values. Fourth, the location accuracy of the phase difference method with h over 30 m is higher than that of the traditional method whether the surrounding medium is fresh water or seawater, except the condition of phase current A with $\sigma = 4$S/m.

In engineering practice, the detection device is usually set on a ship rather than on a UUV in shallow water because of the efficiency, difficulty, and cost of operation. In this case, the detection distance is determined by the water depth. Hence, in some applications with water depths exceeding 30 m, our method helps improve location accuracy by maintaining the original efficiency, difficulty, and cost of operation. Consequently, different methods can be selected based on the different detection distances. When the probe height is within 30 m under the model parameters in this study, the extremum method using the maximum values is a better choice because of its simpler device and criterion. When the probe height is above 30 m, the phase difference method is a better option because of its higher location accuracy.

IV. EXPERIMENTAL SETUP AND RESULTS

Owing to experimental constraints, it is difficult to directly validate the feasibility of the proposed method in seawater. This is because the effects of the amplitude attenuation and phase variation of the magnetic field at 50 Hz in seawater appear as the propagation distance increases. A considerable experimental area with sufficient depth is required to simulate practical applications. In this case, the authors indirectly validate the feasibility of the proposed method in two steps. First, a simple experimental setup is established in air ($\sigma = 0$S/m) rather than seawater ($\sigma = 4$ S/m) to validate the gradient measurement method based on phase difference. From the phase difference detection method discussed above, it is obvious that the method still works whether in air or seawater. The difference is in the location accuracy, where the result in air is close to that in fresh water. Second, the authors compare the phase difference distribution results between the proposed model and the FEM-based model to validate the accuracy of the proposed model. The results for air and seawater are compared.

The coordinate system is consistent with that described in Section II. The experimental setup is shown in Figure 12.

Three parallel straight wires carrying three-phase currents are used to generate the AC magnetic field. A survey line, which is perpendicular to the extended direction of the cables, is set to be consistent with the routing survey of submarine cables in actual engineering [6], [22]. A triaxial fluxgate magnetometer is used to detect the orthogonal components of the magnetic field along the survey line. The distances L_1, L_2, and
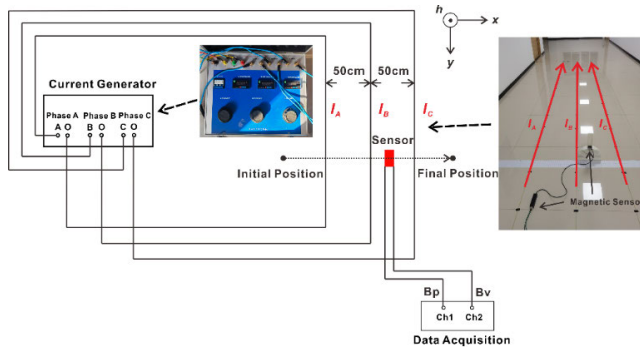
in advance. To compare the location accuracy of the two methods under the effects of detection noise and the surrounding medium, the conditions of the same amplitude noise and different surrounding media are considered. When N_B changes in the range of $0 \sim 1$nT and conductivity (σ) is set to 4S/m, 1 S/m, and 0.01 S/m, respectively, the comparisons of location accuracy are shown in Figure 9 to Figure 11.

In Figure 9 to Figure 11, the dot represents the model bias ($\triangle x$) and the error bar represents the detection error (δ_d). Several conclusions are drawn from this study. First, in most cases, the phase difference method exhibits the smallest detection error, particularly for large h values. This is because of the steep slopes of the phase difference curves near

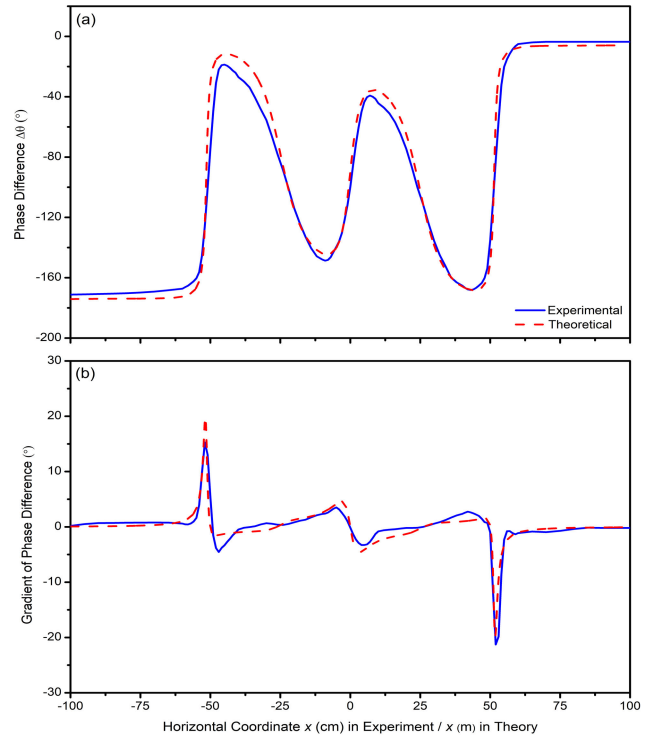**FIGURE 12. The experimental device diagram.**

FIGURE 13. Comparisons between experimental and theoretical results. The blue solid lines represent experimental results and the red dashed lines represent theoretical results. (a) The results of phase difference with the $h = 10$ cm (experimental) and the $h = 10$ m (theoretical). (b) The gradient results of the phase differences in the $h = 10$ cm subtracted from those in the $h = 11$ cm (experimental) and in the $h = 10$ m subtracted from those in the $h = 11$ m (theoretical).

TABLE 1. Details On FEM-based model used.

Parameter	Value or description
Length (X)	300 m
Width (Y)	5 m
Height (Z)	300 m
Cable spacing (L_1 and L_2)	50 m
Balanced phase currents (I_0)	500 A
Cable conductors of phase A, B and C	Copper
Surrounding medium	Air or seawater
Element type	Tetrahedron or triangular prism
Minimum size of element (U_{min})	0.06 m
Maximum size of element (U_{max})	1~10 m

vertical coordinate h are reduced by 100 times compared to the theoretical model discussed earlier. It should be noted that the comparison results are not affected by the reduced space size during the experiment. This is because the wavelength of the 50 Hz AC magnetic field is sufficiently long so that the phase variation with distance (within hundreds of meters) is close to zero in air. Therefore, the effects of proportional reductions in distance L_1, L_2, and vertical coordinate h can be ignored.

The experimental steps are as follows:

Step 1: Set the valid value of the three-phase currents to 1 A using the three-phase current generator.

Step 2: Establish the fluxgate sensor at the initial position $(-100$ cm, 10cm).

Step 3: Simultaneously detect B_p and B_v using the fluxgate sensor and analyze the phase difference data with the data acquisition system.

Step 4: Move the fluxgate sensor along the positive x-axis direction at 1 *cm* intervals.

Step 5: Repeat Steps 3 and 4 until the fluxgate sensor reaches the final position (100 cm, 10cm).

Step 6: Establish the fluxgate sensor at the initial position $(-100$ cm, 11cm).

Step 7: Repeat Steps 3 and 4 until the fluxgate sensor reaches the final position (100 cm, 11cm).

Step 8: Analyze gradient data of phase difference.

The comparisons are shown in Figure 13, indicating that the experimental results are consistent with the theoretical results.

FEM-based modelling is an effective method for further validating the accuracy of the proposed model [23], [24]. The geometry of the FEM-based model is shown in Figure 14, and the conditions are listed in Table 1.

In the FEM-based model, the AC magnetic field is generated by three parallel straight lines carrying the phase currents A, B, and C. The governing equation is as follows:

$$\nabla \times H = J \tag{18}$$

where H is the magnetic field intensity and J is the conduction current density. The boundary condition is set as magnetic insulation, which can be expressed as:

$$n \times A = 0 \tag{19}$$

where n is a normal vector and A is the magnetic vector potential. A comparison of the results from the FEM-based model and the theoretical results of the proposed model in air and seawater is shown in Figure 15. The gradient results are the phase differences in $h = 10$ m subtracted from those in $h = 11$ m.
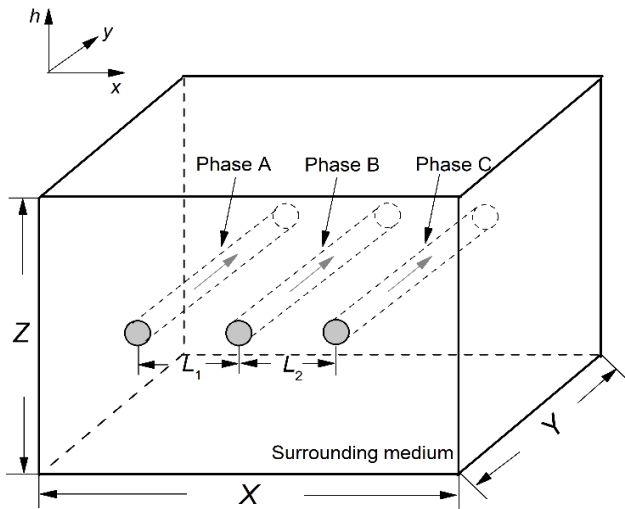
FIGURE 14. The geometry of the FEM-based model. The grey arrows represent the directions of phase currents flow. The origin of coordinate system is set to the geometric center of cuboid.
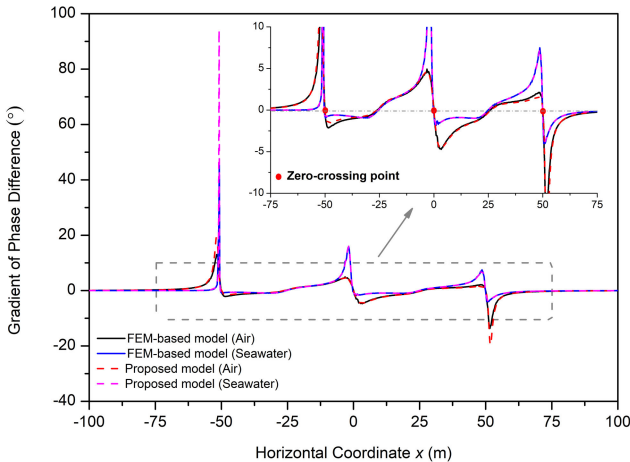

FIGURE 15. Comparisons of phase differences in air and seawater analyzed by the proposed model and FEM-based model. The black solid line represents the result analyzed by FEM-based model in air. The blue solid line represents the result analyzed by FEM-based model in seawater. The red dashed line represents the result analyzed by the proposed model in air. The pink dashed line represents the result analyzed by the proposed model in seawater.

It can be seen that the theoretical results by the proposed model are almost the same with the results by FEM-based model. This validates the accuracy of the proposed model. In addition, the results in air and seawater are different. The result for air is centrosymmetric because the attenuation of the AC magnetic field amplitude with distance is a major factor. In seawater, the phase variation of the AC magnetic field with distance cannot be ignored which causes the results to be different.

To validate the accuracy of the FEM-based model, mesh independence tests are typically used [25], [26], [27]. The results of the mesh independence tests are presented in Figure 16 and Table 2. The phase difference results are analyzed for different element numbers and types.
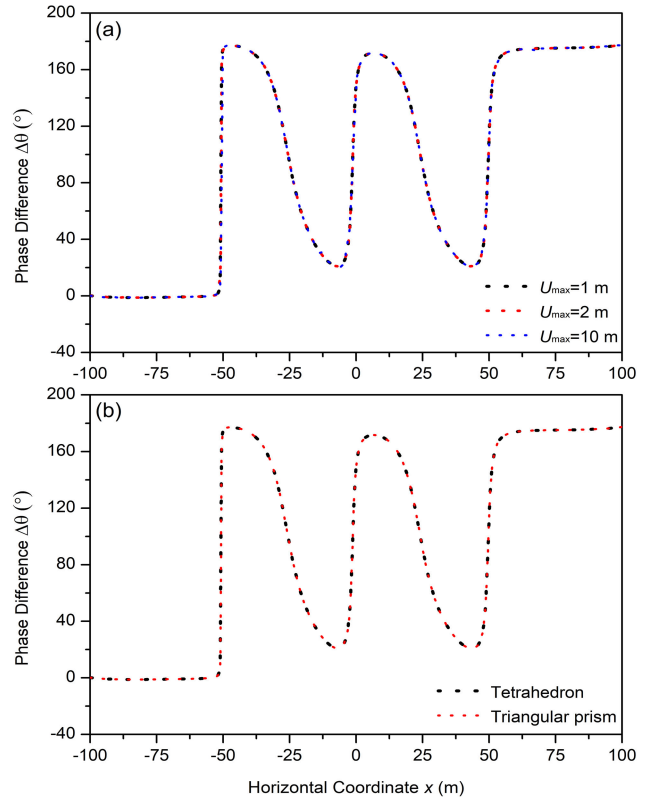

FIGURE 16. Results of the mesh independence tests. (a) The results of different element numbers which are controlled by maximum size of elements (U_{max}). (b) The results of different element types.

TABLE 2. Details on the meshes generated and corresponding mesh independence tests.

| Domain | Finite element mesh Controlled by user | | | | Phase differences at x=0 m in Figure 16 (°) |
	Element type	U_{max} (m)	Number of nodes	Number of elements	
Figure 14	Tetrahedron	10	58471	315105	148.872
Figure 14	Tetrahedron	2	220052	1144852	148.705
Figure 14	Tetrahedron	1	1287300	7669806	148.883
Figure 14	Triangular prism	1	1189474	2149920	148.849

When the maximum size of the element changes from 10 m to 1 m, the element number changes from approximately three hundred thousand to over seven million. This shows that the results are the same whether the element numbers or element types change.

V. CONCLUSION

In this study, the authors develop a general magnetic field model for single-core cables in three-phase submarine power circuits to analyze the impact of mutual magnetic field interference among the cables. By introducing a general magnetic

field model and gradient measurement method based on the phase difference, this study contributes to the understanding of magnetic field variations around submarine power cables and offers a new approach for determining their location. With the parameters ($L_1 = L_2 = 50$ m) discussed in this paper, the authors demonstrate the advantages of phase difference measurements for enhancing location accuracy when the probe height is above 30 m. This means that the traditional method is a better choice because of its simpler device and criterion when the probe height is within the 30 m range. Otherwise, the phase difference method is preferred because of its higher location accuracy. The experimental validation and FEM-based comparisons further support the validity and practicality of the proposed model, paving the way for more accurate and efficient submarine cable detection and maintenance. This method can improve the location accuracy of submarine cables over long distances in practical applications.

ACKNOWLEDGMENT

REFERENCES

[1] B. Taormina, J. Bald, A. Want, G. Thouzeau, M. Lejart, N. Desroy, and A. Carlier, "A review of potential impacts of submarine power cables on the marine environment: Knowledge gaps, recommendations and future directions," *Renew. Sustain. Energy Rev.*, vol. 96, pp. 380–391, Nov. 2018, doi: 10.1016/j.rser.2018.07.026.

[2] C. Kraus and L. Carter, "Seabed recovery following protective burial of subsea cables—Observations from the continental margin," *Ocean Eng.*, vol. 157, pp. 251–261, Jun. 2018, doi: 10.1016/j.oceaneng.2018.03.037.

[3] T. Szyrowski, S. K. Sharma, R. Sutton, and G. A. Kennedy, "Developments in subsea power and telecommunication cables detection: Part 1—Visual and hydroacoustic tracking," *Underwater Technol.*, vol. 31, no. 3, pp. 123–132, Jul. 2013.

[4] H. Matsumoto, E. Araki, T. Kimura, G. Fujie, K. Shiraishi, T. Tonegawa, K. Obana, R. Arai, Y. Kaiho, Y. Nakamura, T. Yokobiki, S. Kodaira, N. Takahashi, R. Ellwood, V. Yartsev, and M. Karrenbach, "Detection of hydroacoustic signals on a fiber-optic submarine cable," *Sci. Rep.*, vol. 11, no. 1, p. 2797, Feb. 2021, doi: 10.1038/s41598-021-82093-8.

[5] K. Sun, W. Cui, and C. Chen, "Review of underwater sensing technologies and applications," *Sensors*, vol. 21, no. 23, p. 7849, Nov. 2021, doi: 10.3390/s21237849.

[6] T. Szyrowski, S. K. Sharma, R. Sutton, and G. A. Kennedy, "Subsea cable tracking in an uncertain environment using particle filters," *J. Mar. Eng. Technol.*, vol. 14, no. 1, pp. 19–31, Jan. 2015, doi: 10.1080/20464177.2015.1022381.

[7] X. Xiang, C. Yu, Z. Niu, and Q. Zhang, "Subsea cable tracking by autonomous underwater vehicle with magnetic sensing guidance," *Sensors*, vol. 16, no. 8, p. 1335, Aug. 2016, doi: 10.3390/s16081335.

[8] T. Szyrowski, S. K. Sharma, R. Sutton, and G. A. Kennedy, "Developments in subsea power and telecommunication cables detection: Part 1—Visual and hydroacoustic tracking," *Underwater Technol.* vol. 31, pp. 123–132, Jul. 2013.

[9] P. Wang, K. F. Goddard, P. L. Lewin, and S. G. Swingler, "Electromagnetic field application to underground power cable detectiom," in *Proc. 17th Int. Symp. High Voltage Eng.*, 2011, pp. 1–5.

[10] A. Fraser-Smith, "Maximum field criteria for a line current source in a conducting medium," *IEEE Trans. Antennas Propag.*, vol. 34, no. 5, pp. 723–725, May 1986, doi: 10.1109/TAP.1986.1143881.

[11] J. Kojima, "Cable tracking by autonomous underwater vehicle," in *Proc. Int. Conf. Phys. Control.*, Cambridge, MA, USA, 2003, pp. 171–174, doi: 10.1109/SSC.2003.1224135.

[12] S. Takagi, J. Kojima, and K. Asakawa, "DC cable sensors for locating underwater telecommunication cables," in *Proc. MTS/IEEE Conf. Coastal Ocean-Prospects 21st Century (OCEANS)*, Fort Lauderdale, FL, USA, vol. 1, Sep. 1996, pp. 339–344, doi: 10.1109/OCEANS.1996.572765.

[13] M. F. Gard, "Magnetic field sensing in the underground construction environment," in *Proc. 2nd ISA/IEEE Sensors Ind. Conf.*, Houston, TX, USA, Nov. 2002, pp. 57–65, doi: 10.1109/SFICON.2002.1159808.

[14] R. G. Olsen and P. S. K. Wong, "Characteristics of low frequency electric and magnetic fields in the vicinity of electric power lines," *IEEE Trans. Power Del.*, vol. 7, no. 4, pp. 2046–2055, Oct. 1992, doi: 10.1109/61.157008.

[15] A. Inan, A. Fraser-Smith, and O. Villard, "ULF/ELF electromagnetic fields produced in a conducting medium of infinite extent by a linear current source of finite length," *IEEE Trans. Antennas Propag.*, vol. AP-33, no. 12, pp. 1363–1369, Dec. 1985, doi: 10.1109/TAP.1985.1143533.

[16] A. A. Abdou, A. Shaw, A. Mason, A. Al-Shamma'a, J. Cullen, and S. Wylie, "Electromagnetic (EM) wave propagation for the development of an underwater wireless sensor network (WSN)," in *Proc. IEEE SENSORS*, Limerick, Ireland, Oct. 2011, pp. 1571–1574, doi: 10.1109/ICSENS.2011.6127319.

[17] A. I. Al-Shamma'a, A. Shaw, and S. Saman, "Propagation of electromagnetic waves at MHz frequencies through seawater," *IEEE Trans. Antennas Propag.*, vol. 52, no. 11, pp. 2843–2849, Nov. 2004, doi: 10.1109/TAP.2004.834449.

[18] M. C. Domingo, "Magnetic induction for underwater wireless communication networks," *IEEE Trans. Antennas Propag.*, vol. 60, no. 6, pp. 2929–2939, Jun. 2012, doi: 10.1109/TAP.2012.2194670.

[19] P. Guofu and Y. Yincan, "Desktop study of site selection for submarine optical cable engineering," in *Submarine Optical Cable Engineering*, Y. Yincan, J. Xinmin, P. Guofu, and J. Wei, Eds. New York, NY, USA: Academic, 2018, ch. 4, pp. 87–115.

[20] L. Lanbo, Z. Shengli, and C. Jun-Hong, "Prospects and problems of wireless communication for underwater sensor networks," *Wireless Commun. Mobile Comput.*, vol. 8, no. 8, pp. 977–994, Oct. 2008.

[21] X. Che, I. Wells, G. Dickers, P. Kear, and X. Gong, "Re-evaluation of RF electromagnetic communication in underwater sensor networks," *IEEE Commun. Mag.*, vol. 48, no. 12, pp. 143–151, Dec. 2010, doi: 10.1109/MCOM.2010.5673085.

[22] Y. Yincan, J. Xinmin, P. Guofu, and J. Wei, "Engineering site survey for submarine optical cable," in *Submarine Optical Cable Engineering*. New York, NY, USA: Academic, 2018, ch. 5, pp. 117–160.

[23] M. Rachek and S. Nait Larbi, "Magnetic eddy-current and thermal coupled models for the finite-element behavior analysis of underground power cables," *IEEE Trans. Magn.*, vol. 44, no. 12, pp. 4739–4746, Dec. 2008, doi: 10.1109/TMAG.2008.2004212.

[24] Z.-Y. Tong, Z.-Y. Dong, and M.-M. Tong, "Analysis of magnetic field generated by overhead cables," *Measurement*, vol. 89, pp. 166–170, Jul. 2016, doi: 10.1016/j.measurement.2016.04.004.

[25] D. Klimenta, D. Tasić, and M. Jevtić, "The use of hydronic asphalt pavements as an alternative method of eliminating hot spots of underground power cables," *Appl. Thermal Eng.*, vol. 168, Mar. 2020, Art. no. 114818, doi: 10.1016/j.applthermaleng.2019.114818.

[26] D. Klimenta, M. Jevtić, D. Andriukaitis, and V. Mijailović, "Increasing the transmission performance of a conventional 110 kV cable line by combining a hydronic concrete pavement system with photovoltaic floor tiles," *Electr. Eng.*, vol. 103, no. 3, pp. 1401–1415, Jun. 2021, doi: 10.1007/s00202-020-01167-4.

[27] Z. Zhang, Y. Luo, Z. Wang, D. Yu, Y. Yang, W. Yan, H. Peng, K. Wu, and W. Yan, "Research on influencing factors of magnetic property test of permanent magnetic ring," *Electr. Eng.*, vol. 104, no. 6, pp. 4071–4080, Dec. 2022, doi: 10.1007/s00202-022-01591-8.

YIRAN CHEN was born in Zhoushan, Zhejiang, China, in 2003. She is currently pursuing the degree with the College of Electronics and Information, Hangzhou Dianzi University, Hangzhou, China.

Her current research interests include magnetic field simulation and detection.

SHANGQING LIANG received the B.S. degree in physics and the Ph.D. degree in optics from Zhejiang University, Hangzhou, China, in 2012 and 2017, respectively.

Since 2017, he has been a Lecturer with the College of Electronics and Information, Hangzhou Dianzi University, Hangzhou. His research interests include optics, atomic and molecular physics, magnetic sensor, and magnetic anomaly detection.

GUOQING YANG received the Ph.D. degree in atomic and molecular physics from the Innovation Academy for Precision Measurement Science and Technology, CAS, Wuhan, China, in 2010.

From 2004 to 2005, he was a Visiting Scholar with Florida International University, FL, USA. He is currently an Associate Professor with the College of Electronics and Information, Hangzhou Dianzi University, Hangzhou, China. His current research interests include quantum optics and magnetic field detection.

LIN WANG received the Ph.D. degree from the Institute of Optics, Department of Physics, Zhejiang University, Hangzhou, China, in 2017.

From 2016 to 2017, she was a Visiting Student with the Institute for Quantum Science and Engineering (IQSE) and the Department of Physics and Astronomy, Texas A&M University, College Station, TX, USA. She is currently an Associate Researcher with Hangzhou Dianzi University. Her current research interests include computational electromagnetics and optics, light propagations in the novel materials, and slow and fast-light propagations.

YUANGUO ZHOU received the Ph.D. degree from the Department of Electronic Science, Institute of Electromagnetics and Acoustics, Xiamen University, Xiamen, China, in 2017.

From 2014 to 2015, he was a Visiting Student with the Department of Electrical and Computer Engineering, Duke University, Durham, NC, USA. From 2015 to 2016, he was a Visiting Student with the Department of Geology and Geophysics, Texas A&M University, College Station, TX, USA. He is currently an Associate Professor with the College of Communication and Information Engineering, Xi'an University of Science and Technology, Xi'an, China. His current research interests include computational electromagnetics and optics, inverse problems, mathematical methods, and deep learning technologies.

XIAOQING TIAN received the M.S. degree in mechanical engineering from Hangzhou Dianzi University, Hangzhou, China, in 2011, and the Ph.D. degree in water conservancy and hydropower engineering from Hohai University, in 2014.

Since 2019, she has been an Associate Professor with the School of Mechanical Engineering, Hangzhou Dianzi University. Her current research interests include marine engineering and hydrodynamics and its applications.

• • •